ISSN 2176-5480

22nd International Congress of Mechanical Engineering (COBEM 2013)
November 3-7, 2013, Ribeirão Preto, SP, Brazil

NONPLANAR VIBRATIONS AND DYNAMIC INSTABILITIES OF GEOMETRICALLY IMPERFECT CANTILEVER BEAMS

E.C. Carvalho
Pontifical Catholic University, Rio de Janeiro, RJ, Brazil
eulher@tecgraf.puc-rio.br

P.B. Gonçalves
Pontifical Catholic University, Rio de Janeiro, RJ, Brazil
paulo@puc-rio.br

Z.J.G.N. Del Prado
Federal University of Goiás, Goiânia, GO, Brazil
zenon@eec.ufg.br

G. Rega
University of Rome, Rome, Italy
giuseppe.rega@uniroma1.it

Abstract. *The aim of this work is to investigate the three-dimensional motions of imperfect cantilever beams under uniformly distributed lateral harmonic excitation. Bifurcations and dynamic instabilities are analyzed near to the 1:1 internal and external resonance regions, by taking into account small geometric imperfections of the beam, which is one of the most important construction factors that influences the nonlinear dynamic behavior of slender bar structures. For this, the nonlinear integro-differential equations describing the flexural-flexural-torsional couplings of the beam are used. All quadratic and cubic nonlinear terms are considered, enough to include the essential inertial and geometric nonlinearities in the formulation. By using the Galerkin procedure, a set of discretized equations of motion are obtained, which are in turn numerically solved by using the Runge-Kutta method. In addition, several tools of nonlinear dynamics are used to determinate and compare the responses of the beam with and without geometric imperfection. The results reveals that the geometric imperfections have a profound influence on the bifurcation scenario and stability of the beam and that, depending on the type and magnitude of the imperfections, the responses for perfect and imperfect beams can be rather different with respect to each other, leading the structure to behaviors unanticipated in the design phase.*

Keywords: *nonplanar vibrations, dynamics instability, flexural-flexural-torsional couplings, bifurcation analysis, geometric imperfections*

1. INTRODUCTION

Due to its high accuracy and capacity to represent both geometric and inertial nonlinearities, the present work is based on the equations of motion derived by Crespo da Silva and coworkers. In 1978 Crepo da Silva and Glynn (1978a and 1978b) presented a set of integro-differential equations able to describe the nonlinear flexural-flexural-torsional coupled motion of inextensible cantilever beams. In the following year, Crespo da Silva and Glynn (1979a), using two of the three equations presented before, studied the influence of possible resonances between the flexural and torsional vibration modes. In another work, published in the same year, Crespo da Silva and Glynn (1979b), applying perturbation technics, studied the nonplanar motion of clamped-clamped beams under uniformly distributed harmonic excitation. One decade later, Crespo da Silva and Zaretzky (1994) used the three integro-differential equations to study the nonlinear nonplanar motion of inextensible cantilever beams, followed by an experimental analysis of the same problem (Zaretzky and Crespo da Silva, 1994).

Nayfeh and Pai (1989) used the two equations formulated by Crepo da Silva and Glynn (1978a and 1978b) to investigate the planar and nonplanar motion of cantilever beams. In 1990, Pai and Nayfeh analyzed the same problem considering a base excitation (Pai and Nayfeh, 1990). At the same time, Luongo *et al.* (1989) studied the nonlinear dynamic behavior of inextensible cantilever beams with open cross section. Some years later, Di Egidio *et al.* (2003a and 2003b) included in the formulation presented by Luongo *et al*. (1989) the deformation of the cross section.

Adopting a beam with closed cross section, Aghababaei *et al.* (2009a), using the hypotheses adopted by Crepo da Silva and Glynn (1978a and 1978b), derived two equations of motion able to describe the nonlinear nonplanar motion of slender inextensible beams with small initial geometric imperfections. In addition, Aghababaei *et al.* (2009b) investigated the nonlinear nonplanar responses of a near-square cantilevered beam with geometric imperfection under harmonic base excitation using the equations presented in Aghababaei *et al.* (2009a).

ISSN 2176-5480

This work aims to investigate the three-dimensional motions of imperfect cantilever beams under uniformly distributed lateral harmonic excitation. First the three equations that govern the flexural-flexural-torsional coupled motion of slender inextensible cantilever beams, including the effect of initial geometric imperfections, are derived. Next, the influence of geometric imperfection on the natural frequencies of the beam is studied. Then, assuming different geometric imperfection shapes and using time histories, Poincaré maps, phase spaces sections, selected cross sections of basin of attraction and bifurcation diagrams, a parametric analysis is conducted to understand the influence of the imperfections in the bifurcation scenario, a problem not tackled in the previous literature on this subject.

2. DYNAMIC SYSTEM

A uniform, homogeneous and inextensible beam of linear isotropic material, length L and mass per unit length m is considered. A deformed beam segment of arc length s is shown in Fig. 1, where the axes (X, Y, Z) define the inertial rectangular coordinate system, while (ξ, η, ζ) denote a local orthogonal curvilinear coordinate system of the beam at the position s in the deformed configuration, which coincide with the principal axes of the beam's cross section. In the perfect configuration, the axes ξ and X are coincident and the axes η and ζ are parallel to the axes Y and Z, respectively. The components of the elastic displacement vector of the centroid C, along the inertial rectangular coordinate system (X, Y, Z), are denoted by $u = u\,(s, t)$, $\overline{v} = \overline{v}\,(s, t) = v + v_0$ and $\overline{w} = \overline{w}\,(s, t) = w + w_0$, where $v = v(s)$ and $w = w(s)$ are the deflections of the beam in the Y and Z directions and $v_0 = v_0(s)$ and $w_0 = w_0(s)$ describe the initial geometric imperfections. In the Fig. 1, $\phi\,(s, t)$ is the angle that describes the orientation of the beam cross section at location s.

To investigate the relative influence of initial geometric imperfections on the nonlinear dynamic behavior of the beam, a square cross section with side length a is adopted in this work, as shown in Fig. 1. The excitation is applied in the Y direction and it is denoted by $Q_v\,(t) = q_v \cos(\Omega_v\, t)$, where q_v is the excitation magnitude, Ω_v is the excitation frequency and t is time.

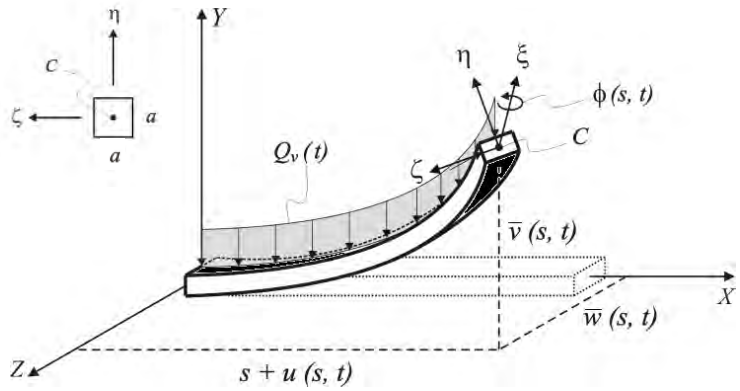

Figure 1. Coordinate systems, displacements, excitation and beam cross section

3. EQUATIONS OF MOTION

Using only one mode approximation in the Galerkin's procedure, the following third-order dimensionless PDEs equations of motion are obtained:

$$
\begin{aligned}
&\left[\left(\int_0^1 F_\gamma^2\,ds\right)+\left(\frac{1}{2}\right)\left(\int_0^1 F_\gamma^2 F_v'^2\,ds\right)\left(v_0^2\right)+\left(\frac{1}{2}\right)\left(\int_0^1 F_\gamma^2 F_w'^2\,ds\right)\left(w_0^2\right)\right]\ddot{\gamma}+\left[\left(c_\gamma\right)\int_0^1 F_\gamma^2\,ds\right]\dot{\gamma}-\left[\beta_\gamma\int_0^1 F_\gamma'' F_\gamma\,ds+\right.\\
&\left.\left(\frac{1}{2}\right)\beta_\gamma\int_0^1\left(F_\gamma F_\gamma' F_v'^2\right)ds\left(v_0^2\right)+\left(\frac{1}{2}\right)\beta_\gamma\int_0^1 F_\gamma F_\gamma' F_w'^2\,ds\left(w_0^2\right)-\int_0^1 F_\gamma^2 F_v''^2\,ds\left(v_0^2\right)-\beta_y\int_0^1 F_\gamma^2 F_w''^2\,ds\left(w_0^2\right)\right]\gamma=\\
&\alpha_{\gamma1}\left(\gamma v^2\right)+\alpha_{\gamma2}\left(\gamma w^2\right)+\alpha_{\gamma3}\left(v w\right)+\left[\alpha_{\gamma4}\left(v w\right)^{\cdot}+\alpha_{\gamma5}\left(v\,\dot{w}\right)\right]^{\cdot}+\alpha_{\gamma6}\left(\gamma\dot{v}^2\right)+\alpha_{\gamma7}\left(\gamma\dot{w}^2\right)+\alpha_{\gamma8}\left(\dot{v}\,\dot{w}\right)+\\
&\alpha_{\gamma9}\left(\gamma v\right)+\alpha_{\gamma10}\left(\gamma w\right)++\alpha_{\gamma11}\left(v^2\right)+\alpha_{\gamma12}\left(w^2\right)+\alpha_{\gamma13}\left(v\right)+\alpha_{\gamma14}\left(w\right)+\left[\alpha_{\gamma15}\left(\dot{v}\right)+\alpha_{\gamma16}\left(\dot{w}\right)\right]^{\cdot},
\end{aligned}
\tag{1}
$$

ISSN 2176-5480

$$\left\{\left(\int_0^1 F_v^2 ds\right)+\left(\frac{1}{2}\right)\left(\int_0^1 F_v'^2 F_v^2 ds\right)\left(v_0^2\right)+\left(\frac{1}{2}\right)\left(\int_0^1 F_w'^2 F_v^2 ds\right)\left(w_0^2\right)-\left(J_\zeta\right)\left(\int_0^1 F_v'' F_v\, ds\right)+\int_0^1 F_v\left(F_v'\int_1^s\int_0^s F_v'^2 ds\, ds\right)' ds\left(v_0^2\right)\right\}\ddot{v}+$$

$$\left[\left(c_v\right)\left(\int_0^1 F_v^2 ds\right)\right]\dot{v}+\left\{\left(\beta_y\right)\left(\int_0^1 F_v^{IV} F_v\, ds\right)-\left(\frac{1}{2}\right)\left(\beta_y\right)\left[\int_0^1 F_v\left(F_v''' F_w'^2\right)' ds\right]\left(w_0^2\right)+\left(\beta_y\right)\int_0^1 F_v\left(F_w'''\int_0^s F_v'' F_w' ds\right)' ds\left(w_0^2\right)+\right.$$

$$\left.\left(\frac{1}{2}\right)\left(\beta_y\right)\int_0^1 F_v\left(F_v''' F_v'^2\right)' ds\left(v_0^2\right)-\left(\beta_y\right)\int_0^1 F_v\left(F_v' F_v''^2\right)' ds\left(v_0^2\right)+\left(1-\beta_y\right)\int_0^1 F_v\left(F_\gamma^2 F_v''\right)'' ds\left(\gamma_0^2\right)\right\} v=\alpha_{v1}(\gamma w)+\alpha_{v2}\left(v\,\gamma^2\right)+$$

$$\alpha_{v3}\left(v\,w^2\right)+\alpha_{v4}\left(v^3\right)+\alpha_{v5}\left[\left(v^2\right)^{\bullet\bullet} v\right]+\alpha_{v6}\left[\left(w^2\right)^{\bullet\bullet} v\right]+\alpha_{v7}\left(v^2\ddot{v}\right)+\alpha_{v8}\left(v w\ddot{w}\right)+\alpha_{v9}\left(\dot{w}\dot{\gamma}\right)+\alpha_{v10}\left(w\dot{v}\dot{w}\right)+\alpha_{v11}\left(v\,\dot{w}^2\right)+ \tag{2}$$

$$\alpha_{v12}\left(\dot{v}\,\gamma^2\right)^{\bullet}+\alpha_{v13}\left(\gamma\ddot{w}\right)+\alpha_{v14}\left(v\dot{v}^2\right)+\alpha_{v15}(\gamma)+\alpha_{v16}(v w)+\alpha_{v17}\left(w^2\right)+\alpha_{v18}\left(\dot{v}\dot{w}\right)+\alpha_{v19}\left(\dot{w}^2\right)+\alpha_{v20}\left(v\ddot{w}\right)+\alpha_{v21}\left(w\ddot{w}\right)+$$

$$\alpha_{v22}\left(v^2\right)+\alpha_{v23}(w)+\alpha_{v24}\left(\gamma^2\right)+\alpha_{v25}(\gamma v)+\alpha_{v26}\left(v\ddot{v}\right)+\alpha_{v27}\left(w^2\right)^{\bullet\bullet}+\alpha_{v28}\left(v^2\right)^{\bullet\bullet}+\alpha_{v29}\left(\ddot{w}\right)+\alpha_{v30}\left(w\dot{\gamma}\right)+$$

$$\int_0^1 q_v(s)\cos(\Omega t)\left[F_v+\left(\frac{1}{2}\right)\left(F_v'^2 F_v\right)\left(v_0^2\right)+\left(\frac{1}{2}\right)\left(F_w'^2 F_v\right)\left(w_0^2\right)\right] ds\,,$$

$$\left\{\left(\int_0^1 F_w^2 ds\right)+\left(\frac{1}{2}\right)\left(\int_0^1 F_v'^2 F_w^2 ds\right)\left(v_0^2\right)+\left(\frac{1}{2}\right)\left(\int_0^1 F_w'^2 F_w^2 ds\right)\left(w_0^2\right)-\left(J_\eta\right)\left(\int_0^1 F_w'' F_w\, ds\right)+\int_0^1 F_w\left(F_w'\int_1^s\int_0^s F_w'^2 ds\, ds\right)' ds\left(w_0^2\right)\right\}\ddot{w}+$$

$$\left[\left(c_w\right)\left(\int_0^1 F_w^2 ds\right)\right]\dot{w}+\left\{\left(\int_0^1 F_w^{IV} F_w\, ds\right)-\left(\frac{1}{2}\right)\left[\int_0^1 F_w\left(F_w''' F_v'^2\right)' ds\right]\left(v_0^2\right)+\int_0^1 F_w\left(F_v'''\int_0^s F_v'' F_w' ds\right)' ds\left(v_0^2\right)-\right.$$

$$\left.\left(\frac{1}{2}\right)\int_0^1 F_w\left(F_w''' F_w'^2\right)' ds\left(w_0^2\right)+\int_0^1 F_w\left[F_w'\left(F_w' F_w''\right)'\right]' ds\left(w_0^2\right)-\left(1-\beta_y\right)\int_0^1 F_w\left(F_\gamma^2 F_w''\right)'' ds\left(\gamma_0^2\right)\right\} w=\alpha_{w1}(\gamma v)+\alpha_{w2}\left(w\,\gamma^2\right)+ \tag{3}$$

$$\alpha_{w3}\left(w\,v^2\right)+\alpha_{w4}\left(w^3\right)+\alpha_{w5}\left[\left(w^2\right)^{\bullet\bullet} w\right]+\alpha_{w6}\left[\left(v^2\right)^{\bullet\bullet} w\right]+\alpha_{w7}\left(w^2\ddot{w}\right)+\alpha_{w8}\left(v w\ddot{v}\right)+\alpha_{w9}\left(\dot{v}\dot{\gamma}\right)+\alpha_{w10}\left(v\dot{v}\dot{w}\right)+\alpha_{w11}\left(w\,\dot{v}^2\right)+$$

$$\alpha_{w12}\left(\dot{w}\,\gamma^2\right)^{\bullet}+\alpha_{w13}\left(\gamma\ddot{v}\right)+\alpha_{w14}\left(w\dot{w}^2\right)+\alpha_{w15}(\gamma)+\alpha_{w16}(v w)+\alpha_{w17}\left(v^2\right)+\alpha_{w18}\left(\dot{v}\dot{w}\right)+\alpha_{w19}\left(\dot{v}^2\right)+\alpha_{w20}\left(w\ddot{v}\right)+\alpha_{w21}\left(v\ddot{v}\right)+$$

$$\alpha_{w22}\left(w^2\right)+\alpha_{w23}(v)+\alpha_{w24}\left(\gamma^2\right)+\alpha_{w25}(\gamma w)+\alpha_{w26}\left(w\ddot{w}\right)+\alpha_{w27}\left(v^2\right)^{\bullet\bullet}+\alpha_{w28}\left(w^2\right)^{\bullet\bullet}+\alpha_{w29}\left(\ddot{v}\right),$$

Details of this formulation, not considering the initial geometric imperfection, can be found in Crespo da Silva (1991), where $\gamma = \gamma(t)$ is the angle of torsion, β_y and β_γ are nondimensional stiffness parameters, J_η and J_ζ are the moments of inertia and c_v, c_w and c_γ, are the linear viscous damping coefficients. The superscript (') denotes partial differentiation with respect to s and the superscript ($^\bullet$) means differentiation with respect to time t. Finally, the eigenfunctions $F_v(s)$, $F_w(s)$ and $F_\gamma(s)$ used in the Galerkin procedure have the following form:

$$F_{v,w}=C_{v,w}\left\{\cosh\left(r_{1,3}\,s\right)-\cos\left(r_{2,4}\,s\right)-K_{v,w}\left[\sinh\left(r_{1,3}\,s\right)-\left(r_{1,3}/r_{2,4}\right)\sin\left(r_{2,4}\,s\right)\right]\right\}, \tag{4}$$

$$F_\gamma=C_\gamma\sin\left[(\pi/2)s\right], \tag{5}$$

where the quantities r_1 to r_4 are obtained from the solution of the characteristic equation,

$$r_{1,3}^4+r_{2,4}^4+2r_{1,3}^2 r_{2,4}^2\cosh\left(r_{1,3}\right)\cos\left(r_{2,4}\right)+r_{1,3}\,r_{2,4}\left(r_{2,4}^2-r_{1,3}^2\right)\sinh\left(r_{1,3}\right)\sin\left(r_{2,4}\right)=0\,, \tag{6}$$

In the above equations α_{vi}, α_{wi} e $\alpha_{\gamma i}$ (for i = 1, 2, 3, …) are the Galerkin's coefficients, which can be found in Carvalho (2013).

ISSN 2176-5480

4. NONLINEAR VIBRATION

To investigate the influence of possible initial geometric imperfections on the nonlinear dynamic behavior of highly flexible slender structures, a cantilever beam with square cross section of relative size $a/L = 25$ is adopted (see Fig. 1). For this geometry, $\beta_y = 1.0$, $\beta_\gamma = 0.643810$, $J_\eta = J_\zeta = 0.000133$, $J_\xi = 0.000266$, $C_v = C_w = 1.0$ e $C_\gamma = 1.414214$. Replacing these values in Eqs. (1) to (3), the following set of discretized equations of motion is obtained:

$$\begin{aligned}&\left[1.0000+3.2517\left(v_0^2+w_0^2\right)\right]\ddot{\gamma}+1.0000c_\gamma\dot{\gamma}+\left[5957.0112+6116.5163\left(v_0^2+w_0^2\right)\right]\gamma+\\&2.6746\left(\ddot{v}\,w-\ddot{w}v+w_0\,\ddot{v}-v_0\,\ddot{w}\right)+12054.5346\left(v_0\,\gamma v+w_0\,\gamma w\right)-16227.3797\left(w_0\,v+v_0\,w\right),\end{aligned} \tag{7}$$

$$\begin{aligned}&\left(1.0001+8.1718v_0^2+3.5727w_0^2\right)\ddot{v}+1.0002c_v\dot{v}+\left(12.3653-50.5787v_0^2\right)v-4.2487\gamma w+\\&40.4629\left(vw^2+v^3+v_0\,w^2\right)+4.5991\left[\left(\dot{v}^2+v\ddot{v}+\dot{w}^2+w\ddot{w}\right)\left(v+v_0\right)+v_0\,w_0\,\ddot{w}+w_o\,v\,\ddot{w}+v_0\,v\,\ddot{v}\right]-\\&0.0017\left(v^2\,\ddot{v}+vw\ddot{w}+w\dot{w}\dot{v}+v\dot{v}^2+w_0\,\dot{v}\dot{w}-v_0\,\dot{w}^2\right)+0.7919\,w_0\,\gamma-30.3472w_0\,v\,w+91.0416v_0v^2+\\&50.5787v_0\,w_0\,w+1.6073v_0\,\gamma^2-0.0007\left(\dot{w}\dot{\gamma}-c_\gamma\,w\dot{\gamma}\right)-\left[0.7831+3.5727\left(w_0^2+v_0^2\right)\right]q_v\cos\left(\Omega_v\,t\right),\end{aligned} \tag{8}$$

$$\begin{aligned}&\left(1.0001+8.1718w_0^2+3.5727v_0^2\right)\ddot{w}+1.0002c_w\dot{w}+\left(12.3653-50.5787\,w_0^2\right)w+4.2487\gamma v+\\&40.4629\left(wv^2+w^3+w_0\,v^2\right)+4.5991\left[\left(\dot{w}^2+w\ddot{w}+\dot{v}^2+v\ddot{v}\right)\left(w+w_0\right)+w_0\,v_0\,\ddot{v}+v_0\,w\ddot{v}+w_0\,w\ddot{w}\right]-\\&0.0017\left(w^2\,\ddot{w}+wv\ddot{v}+v\dot{v}\dot{w}+w\dot{w}^2+v_0\,\dot{w}\dot{v}-w_0\,\dot{v}^2\right)-0.7919\,v_0\,\gamma-30.3472v_0\,w\,v+91.0416w_0\,w^2+\\&50.5787w_0\,v_0\,v+1.6073w_0\,\gamma^2-0.0007\dot{v}\dot{\gamma}\,.\end{aligned} \tag{9}$$

Linearizing Eqs. (7) to (9), the three natural frequencies of the beam are obtained as a function of the geometric imperfections v_0 and w_0. They are:

$$\omega_v^2=\frac{12.3653-50.5787\,v_0^2}{1.0001+8.1718\,v_0^2+3.5727\,w_0^2}\,, \tag{10}$$

$$\omega_w^2=\frac{12.3653-50.5787\,w_0^2}{1.0001+8.1718\,w_0^2+3.5727v_0^2}\,, \tag{11}$$

$$\omega_\gamma^2=\frac{5057.0112+6116.5163\left(v_0^2+w_0^2\right)}{1.0000+3.2517\left(v_0^2+w_0^2\right)}\,. \tag{12}$$

Figure 2 shows the variation of the natural frequency of the beam as a function of the geometric imperfection magnitude.

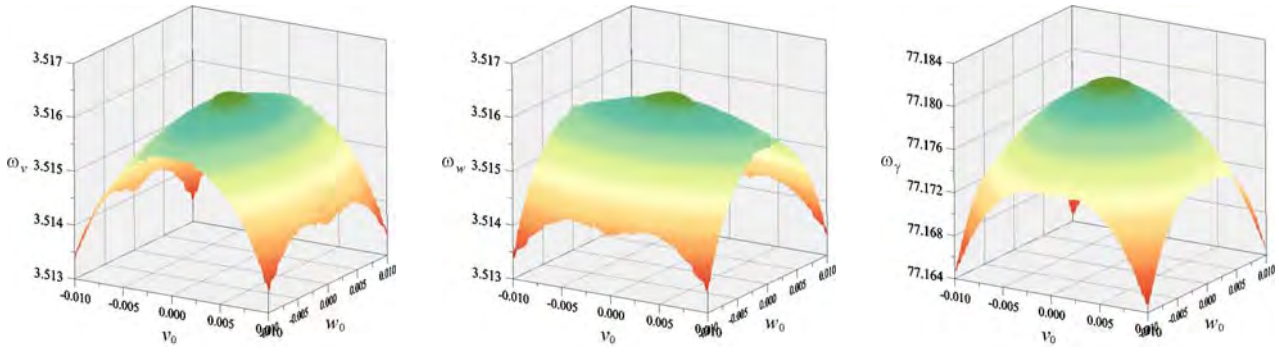

(a) Surface v_0 vs. w_0 vs. ω_v (b) Surface v_0 vs. w_0 vs. ω_w (c) Surface v_0 vs. w_0 vs. ω_γ

Figure 2. Influence of the imperfections on the natural frequencies of the beam

ISSN 2176-5480

Comparing the Fig. 2a with the Fig 2b, it is observed that one is a mirror image from the other, i.e., a point with coordinates (v_0, w_0, ω_v) in Fig. 2a correspond to a point with coordinates (w_0, v_0, ω_w) in Fig. 2b. So, the 1:1 internal resonance ($\omega_v = \omega_w$) can be observed whenever the module of v_0 is equal to the module of w_0. As observed here, all natural flexural frequencies decrease with the geometric imperfections. For this cross section geometry the torsional frequency is much higher than the flexural natural frequencies. Based in this system characteristic, most of the works in this research area disregards the angle of torsion, adopting a system with only two degrees of freedom (2DOF). Here no simplification is considered.

5. FORCED MOTION

The forced and damped motion of beam is studied now, considering a uniformly lateral harmonic excitation denoted by $q_v \cos(\Omega_v t)$ and applied in the Y direction (see Fig. 1). An excitation magnitude $q_v = 0.025$ and linear viscous damping $c_v = c_w = c_\gamma = 0.6\%$ are adopted. The bifurcation diagram in the Ω_v vs. v vs. w space, for the perfect beam ($v_0 = w_0 = 0.0$), is shown in Fig. 3.

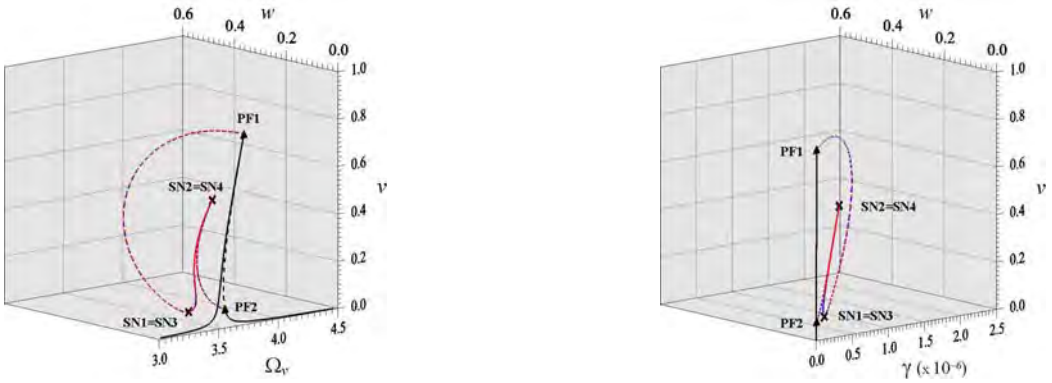

(a) Projection Ω_v vs. v vs. w

(b) Projection γ vs. v vs. w

Figure 3. Bifurcation diagrams for the perfect beam

Here the maximum displacement of the beam is plotted as a function of the excitation frequency. These bifurcation diagrams were obtained by using the continuation software AUTO (Doedel *et al.*, 1998). The continuous curves correspond to the stable solutions and dashed curves to the unstable solutions. To facilitate the parametric analysis, different colors are used for different solutions branches. The black curve, corresponds to the in-plane vibrations of the beam (classical resonance curve), where load and structure are contained in the same plane (the displacement w and the angle of torsion γ are equal to zero). Due to the modal coupling, the displacement w and the angle of torsion γ are excited and two new branches of solutions appear (blue and red branches) connecting the subcritical pitchfork bifurcation points PF1 and PF2. They are coincident due to the symmetry of the cross section with relation to the load direction. This means that the same vibration pattern is observed for both bifurcated branches (one exhibiting a clockwise and the other a counterclockwise motion). Along these new bifurcated branches saddle-node bifurcations occur with stable solution branches between SN1 = SN3 and SN2 = SN4. This leads to several coexisting attractors in the main resonance region associated with planar and non-planar motions.

Figures 4 and 5 show the bifurcation diagrams for the beam with, respectively, initial geometric imperfection $v_0 = 0.01$ (0.04% L) and $w_0 = 0.01$. Comparing the projections of these two diagrams with Fig. 3, important differences can be observed. In the Fig. 4a (see detail in Fig. 4c) it is observed that the subcritical pitchfork bifurcation point PF1 moves along the previously unstable branch of planar motions prolonging the stable region and creating an additional stable coexisting solution. In the Fig. 5a (see detail in Fig. 5c), however, the pitchfork bifurcation point PF1 moves in the opposite direction, increasing the unstable region, and the pitchfork bifurcation becomes supercritical, leading to a different sequence of stable and unstable branches of non-planar solutions (blue and red). Two new saddle-node bifurcation point appear (NS5=NS6), with stable solutions between the points PF1 and SN5=SN6 and SN1=SN3 and SN2=SN4. Additionally, the nonplanar solution branches, coincident in the perfect case (Fig. 3), start to diverge from each other, as shown in Fig. 4 and Fig. 5. This behavior occurs due to the symmetry breaking effect imposed by the geometric imperfections.

To clarify the strong influence of the geometric imperfections on the dynamic behavior of the beam, Fig. 6 and Fig. 7 show some time histories, phase space projections and Poincaré maps for, respectively, $v_0 = 0.01$ and $w_0 = 0.01$, considering $\Omega_v = 3.66064$. The solutions refer to Fig. 4 and Fig. 5, following the same color convention. These projections are observed in the hyperplane defined by $\dot{v} = 1.881350$, $\dot{w} = -0.470302$, $\gamma = 0.011297$ and $\dot{\gamma} = 0.051874$.

ISSN 2176-5480

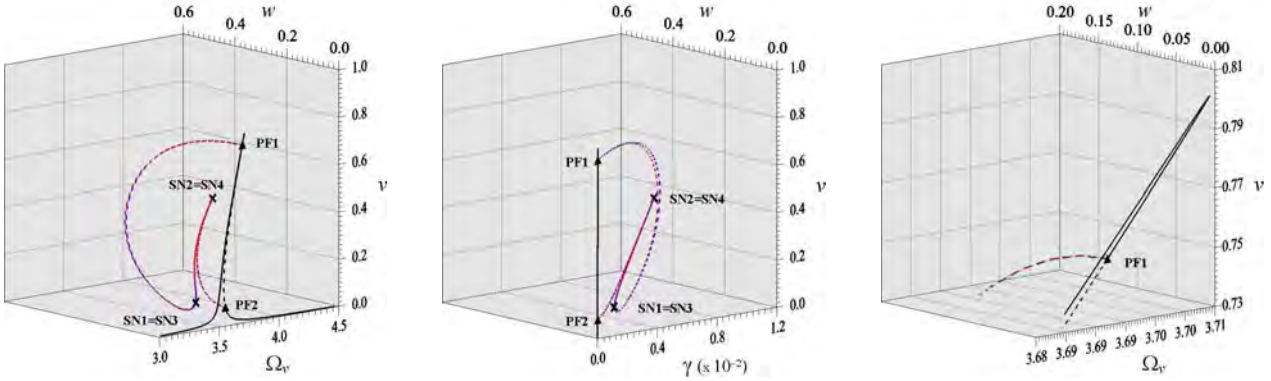

(a) Projection Ω_v vs. v vs. w (b) Projection γ vs. v vs. w (c) Detail of the projection Ω_v vs. v vs. w at the PF1 bifurcation region

Figure 4. Bifurcation diagrams for the beam with initial geometric imperfection $v_0 = 0.01$

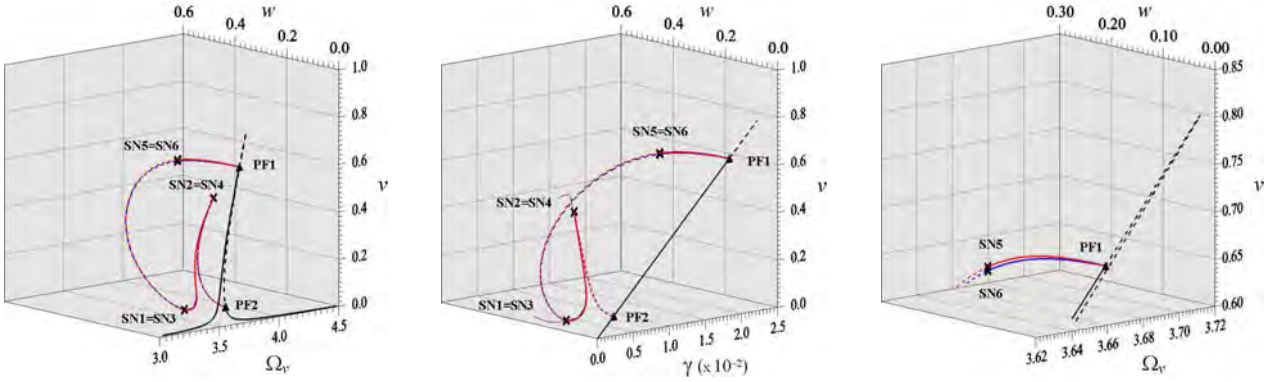

(a) Projection Ω_v vs. v vs. w (b) Projection γ vs. v vs. w (c) Detail of the projection Ω_v vs. v vs. w at the PF1 bifurcation region

Figure 5. Bifurcation diagrams for the beam with initial geometric imperfection $w_0 = 0.01$

Figure 6 shows four period one stable solutions (four fixed points in Fig. 6c, each one associated with a closed orbit in the phase space projection). Two planar solutions (the small amplitude solution TS and the large amplitude solution TL) and two non-planar solutions (NT1 and NT2) are observed. Comparing the Fig. 6 with the Fig. 7, one can observed that when $\Omega_v = 3.66064$ the large amplitude planar solution disappears and two period one nonplanar additional solutions are observed (NT3 and NT4), which arise in the state variable space when the imperfection occurs orthogonal to the excitation plane, i.e., in the Z direction ($w_0 = 0.01$.

Additionally, Fig. 6d and 7d show the deformed beam configuration for, respectively, the four and five possible stable equilibrium configuration. Among these possible coexisting solutions, that assumed by the structure depends on of the system initial conditions.

Some v vs. w cross sections of the six dimensional basin of attraction are presented in the Fig. 8 for $v_0 = 0.01$, and in the Fig. 9 for $w_0 = 0.01$ (see detail in Fig. 9b), both defined by the $\dot{v} = 1.881350$, $\dot{w} = -0.470302$, $\gamma = 0.011297$, $\dot{\gamma} = 0.051874$ hyperplane. In these sections, six different regions, each one associated with a specific behavior, are observed. They are: (a) black region – solution with large vibrations occurring in the same plane as the excitation (TL in Fig. 6), (b) gray region – solution with small vibrations occurring in the same plane as the excitation (TS in Fig. 6 and Fig. 7), (c) blue and red regions – nonplanar solutions excited due to the modal coupling and with moderate vibration amplitude (respectively, NT2 and NT1 in Fig, 6 and Fig. 7) and (d) dark blue and dark red regions – nonplanar solutions with large vibration amplitude (respectively, NT3 and NT4 in Fig. 7). The yellow dots are projections of the fixed points of the Poincaré map onto the chosen cross sections.

A well-defined set of initial conditions is identified in Fig. 8, which lead to vibrations with large amplitude in the same plane as the excitation (black region). A great sensibility to initial conditions is observed in the remaining basin, with non-planar sub-basins (blue and red) intercalated by the planar gray basin associated with the small amplitude planar solution. A fractal basin is also observed in the Fig. 9, where a very small set of initial conditions associated with the dark blue and dark red sub-basins can be identified in Fig. 9b.

ISSN 2176-5480

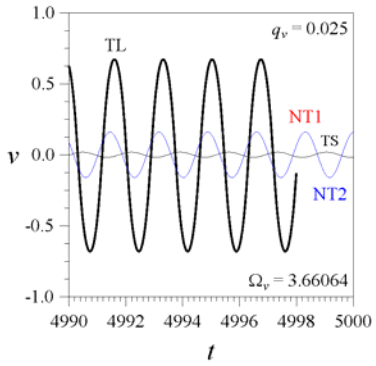

(a) *v* vs. *t* time history

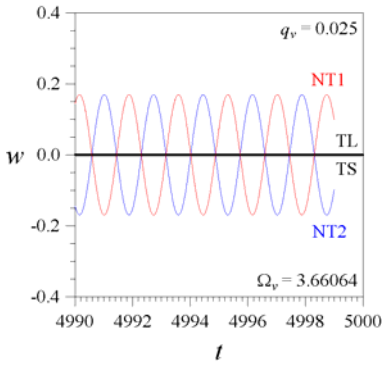

(b) *w* vs. *t* time history

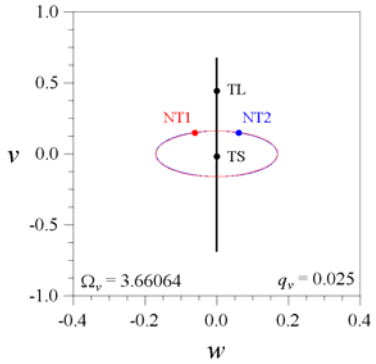

(c) *v* vs. *w* phase space projection and Poincaré map (dots)

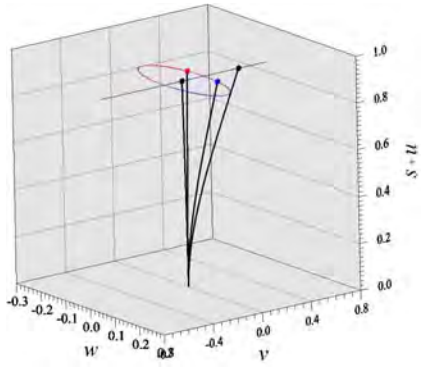

(d) (*s* + *u*) vs. *v* vs. *w* phase space projection and deformed configuration

Figure 6. Coexisting stable solutions for Ω_v = 3.66064 and v_0 = 0.01

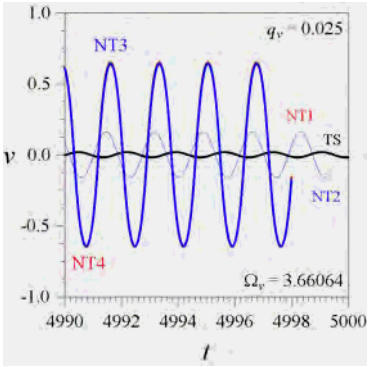

(a) *v* vs. *t* time history

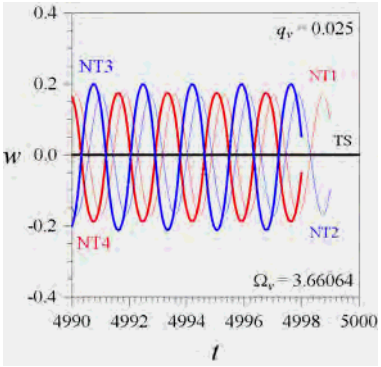

(b) *w* vs. *t* time history

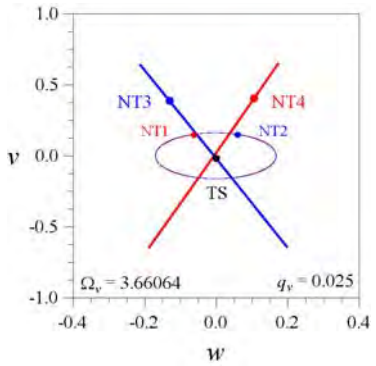

(c) *v* vs. *w* phase space projection and Poincaré map

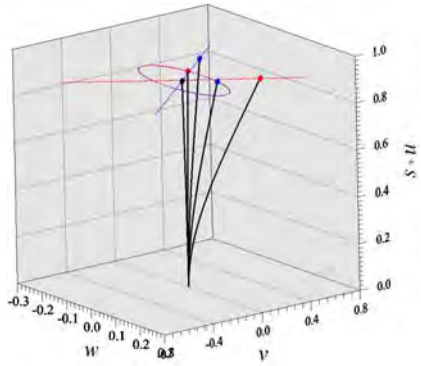

(d) (*s* + *u*) vs. *v* vs. *w* phase space projection and deformed configuration

Figure 7. Coexisting stable solutions for Ω_v = 3.66064 and w_0 = 0.01

ISSN 2176-5480

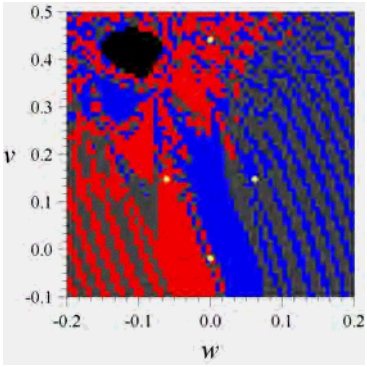

Figure 8. v vs. w cross section of the basin of attraction for $\dot{v}$ = 1.881350, $\dot{w}$ = -0.470302, γ = 0.011297 and $\dot{\gamma}$ = 0.051874, considering Ω_v = 3.66064 and v_0 = 0.01

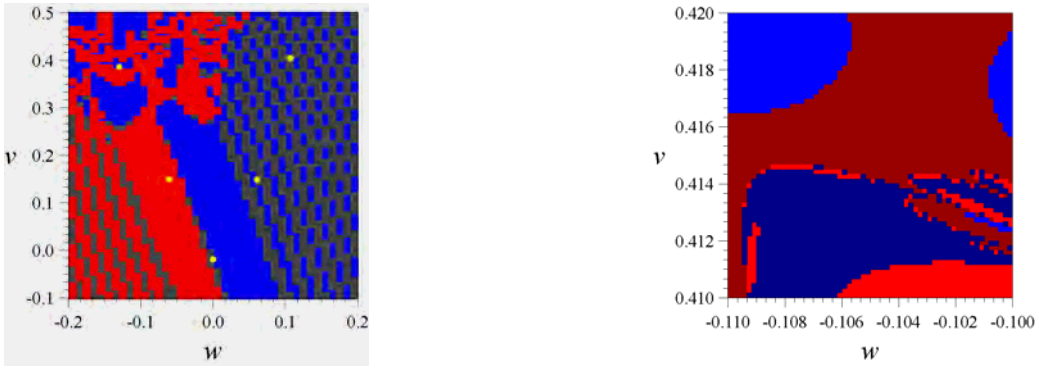

(a) Seção v vs. w

(b) Detalhe da projeção v vs. w

Figure 9. v vs. w cross section of the basin of attraction for $\dot{v}$ = 1.881350, $\dot{w}$ = -0.470302, γ = 0.011297 and $\dot{\gamma}$ = 0.051874, considering Ω_v = 3.66064 and w_0 = 0.01

The results presented up to this point of the work are already enough to give a good illustration about the strong influence of geometric imperfections on the dynamic behavior of slender cantilever beams, changing the bifurcation scenario of the structure and, due to that, leading the system to new periodic solutions, including some with large vibration amplitude. Furthermore, is observed that the direction of the imperfection, with respect to the excitation direction, also has a profound influence on the instabilities of the system.

Considering this last point in view, a geometric imperfection at 45º, with $v_0 = w_0 = 0.001$ (very small imperfection), is imposed on the system. In the Fig. 10a it is observed that the solutions associated with the black curve are no longer planar and the pitchfork bifurcation point PF1 moves out of the Ω_v vs. v plane. Also the two non-planar solution branches (blue and red), due to the simultaneous imperfections ($v_0 = w_0$) considered, are no longer coincident (see Fig. 10b). However, considering the higher geometric imperfection magnitude, $v_0 = w_0 = 0.01$, a profound change can be observed on the response of the structure (Fig. 11). For this geometric imperfection magnitude, the response diverges radically from the classical resonance curve, giving rise to a new non-planar solution branch (green with $w \neq 0.0$ and $\gamma \neq 0.0$) and the pitchfork bifurcation point PF1 disappear, arising in its place a new saddle-node bifurcation point (SN0).

At this point, it is important call attention to the fact that, the angle of torsion, not considered in previous works on beams with high torsional stiffness, in addition to providing additional information on the three dimensional motions of the beam, becomes indispensable when the vibrations reach large amplitudes. Fig. 12, e.g., shows a bifurcation diagram for the beam with geometric imperfections $v_0 = w_0 = 0.01$, obtained disregarding the angle of torsion ($\gamma = 0$) in the Eqs. (7) to (9), i.e., considering a system with only 2DOF (v and w). To help in the comparison, Fig. 12 also shows, in gray, the bifurcation diagram presented before in the Fig. 11. It is observed that the response of the structure obtained considering a system with 2DOF is different from that obtained considering a 3DOF system (v, w and γ). This difference is also observed looking at the phase space projection, together with the Poincaré map, in the Fig. 12b for a solution with large amplitude. Thus, the traditional 2DOF system used for perfect bar structures with large torsional stiffness cannot be used to study beams with initial geometric imperfections.

ISSN 2176-5480

Finally, to complement the numerical results presented in this work, the bifurcation diagrams considering $v_0 = 2\ w_0 = 0.01$ and $w_0 = 2\ v_0 = 0.01$ are shown in Fig. 13a and Fig. 13b, respectively, where the influence of the geometric imperfections on the response of the structure can be observed again.

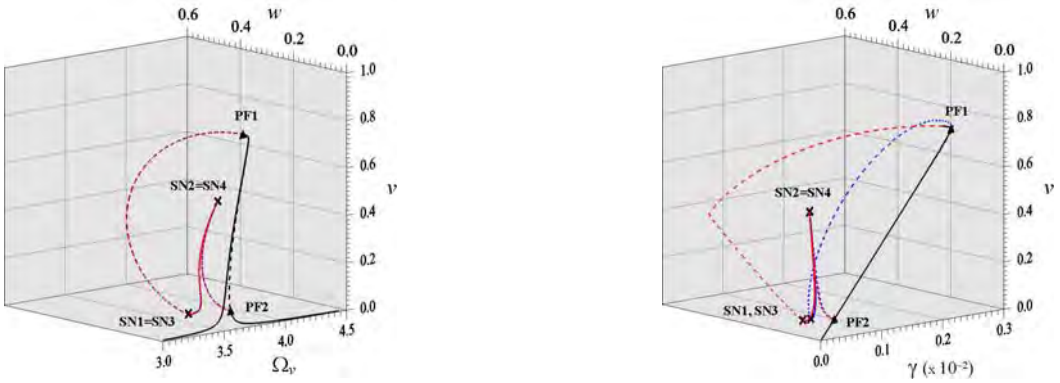

(a) Projection Ω_v vs. v vs. w (b) Projection γ vs. v vs. w

Figure 10. Bifurcation diagrams for the beam with initial geometric imperfection $v_0 = w_0 = 0.001$

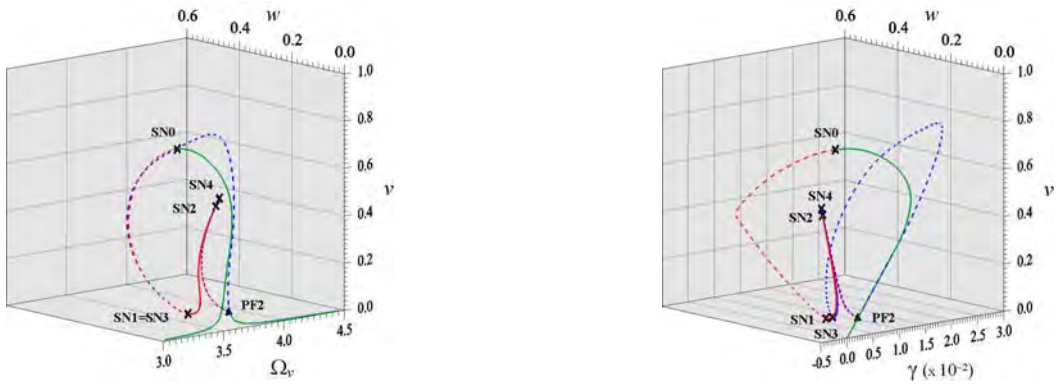

(a) Projection Ω_v vs. v vs. w (b) Projection γ vs. v vs. w

Figure 11. Bifurcation diagrams for the beam with initial geometric imperfection $v_0 = w_0 = 0.01$

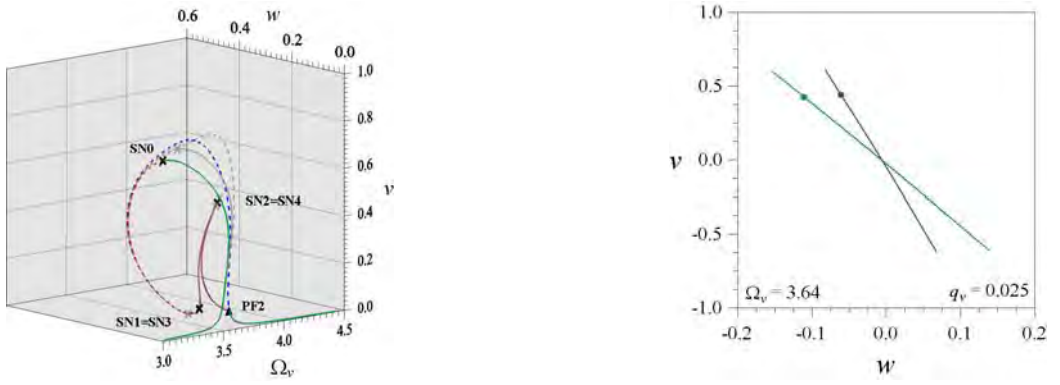

(a) Ω_v vs. v vs. w bifurcation diagram projection (b) v vs. w phase space projection

Figure 12. Bifurcation diagrams and phase space projection for the beam with initial geometric imperfection $v_0 = w_0 = 0.01$, obtained considering $\gamma = 0.0$ in the Eqs. (7) to (9)

In particular, due to the difference between the geometric imperfection components ($v_0 \neq w_0 \neq 0.0$) and the resulting asymmetry, a different sequence of bifurcation can be observed in each case. In particular, in Fig. 13b, four new saddle-node bifurcation points appear (SN5=SN7 and SN6=SN8), changing consequently the stability of the solutions and the number of coexisting solutions for a given forcing frequency.

ISSN 2176-5480

6. CONCLUSIONS

The flexural-flexural-torsional response of slender cantilever beams was investigated in this work by taking into account the effect of initial geometric imperfection. Both geometrical and inertial nonlinearities were considered in the equations of motion. The beams were subjected to a uniformly distributed lateral harmonic excitation.

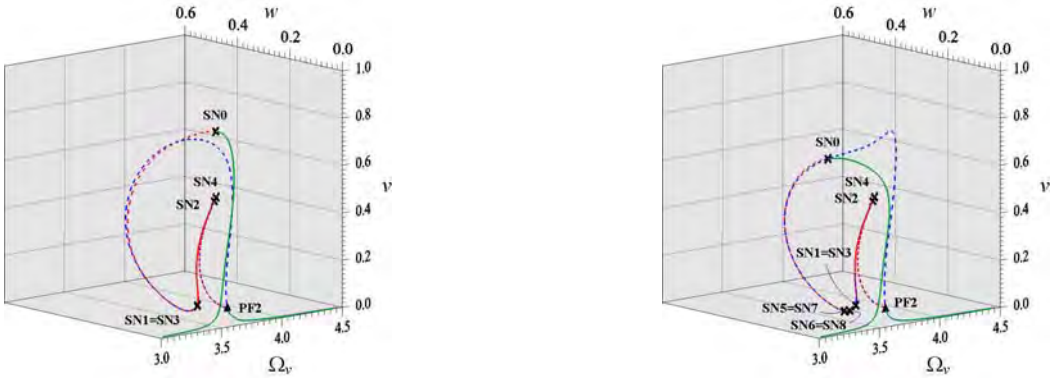

(a) Ω_v vs. v vs. w projection, assuming $v_0 = 2$ $w_0 = 0.01$

(b) Ω_v vs. v vs. w projection, assuming $w_0 = 2$ $v_0 = 0.01$

Figure 13. Bifurcation diagrams for the beam with initial geometric imperfection $v_0 \neq w_0 \neq 0.0$

Numerical integration of the equations of motion and bifurcation diagrams were used to investigate the behavior of the beam. The results show a remarkable influence of geometric imperfections on the dynamics behavior of structure, changing the bifurcation scenario of the beam and leading the system to different planar and nonplanar periodic solutions with small, moderate and large vibration amplitudes. Also, the results show that the traditional 2DOF systems used for perfect bar structures with large torsional stiffness cannot be used to study beams with initial geometric imperfections, being necessary to include in the formulation the torsion angle (3DOF system). Finally, the results call attention to the need for a careful design of tall self-supported towers and mast and similar structural systems working in a dynamic environment.

7. ACKNOWLEDGEMENTS

The authors acknowledge the support of FAPERJ, CAPES and CNPq.

8. REFERENCES

Aghababaei, O., Nahvi, H. and Ziaei-Rad, S., 2009a. “Non-linear non planar vibrations of geometrically imperfect inextensional beams, part I: equations of motion and experimental validation”. *International Journal of Non-Linear Mechanics*. Vol. 44, p. 147-160.

Aghababaei, O., Nahvi, H. and Ziaei-Rad, S., 2009b. “Non-linear non-planar vibrations of geometrically imperfect inextensional beams, Part II: Bifurcations analysis under base excitations”. *International Journal of Non-Linear Mechanics*. Vol. 44, No. 2, p. 160-178.

Carvalho, E. C., 2013. *Nonlinear and Non-planar Vibrations and Dynamic Instability of Slender Bars*. D.Sc. Thesis, PUC-Rio, Rio de Janeiro, Brazil.

Crespo da Silva, M.R.M. and Glynn, C.C., 1978a. “Nonlinear flexural-flexural-torsional dynamics of inextensional beams. I. Equation of motion”. *Journal of Structural Mechanics*, Vol. 6, p. 437-438.

Crespo da Silva, M.R.M. and Glynn, C.C., 1978b. “Nonlinear flexural-flexural-torsional dynamics of inextensional beams. II. Forced motion”. *Journal of Structural Mechanics*. Vol. 6, p. 449-461.

Crespo da Silva, M.R.M. and Glynn, C.C., 1979a. “Nonlinear nonplanar resonant oscillations in fixed-free beams with support asymmetry”. *International Journal of Solids and Structures*. Vol. 15, p. 209-219.

Crespo da Silva, M.R.M. and Glynn, C.C., 1979b. “Out-of-plane vibrations of a beam including non-linear inertia and non-linear curvature effects”. *Non-Linear Mechanics*. Vol. 13, p. 261-271.

Crespo da Silva, M.R.M. and Zaretzky, C.L., 1994. “Nonlinear flexural-flexural-torsional interections in beams including the effect of torsional dynamics. I. Primary resonance”. *Nonlinear Dynamics*. Vol. 5, p. 3-23.

Crespo da Silva, M.R.M., 1991, “Equations for nonlinear analysis of 3d motions of beans”. *Applied Mechanics Reviews*. Vol. 44, pp. 51-59.

Di Egidio, A., Luongo, A. and Vestroni, F., 2003a. “A non-linear model for the dynamics of open cross-section thin-walled beams – Part I: formulation”. *Nonlinear mechanics*. Vol. 38, p. 1067-1081.

ISSN 2176-5480

Di Egidio, A., Luongo, A. and Vestroni, F., 2003b. “A non-linear model for the dynamics of open cross-section thin-walled beams – Part II: forced motion”. *Nonlinear mechanics*. Vol. 38, p. 1083-1094.

Doedel, E. J., Champneys, A. R., Fairgrieve, T. F., Kuznetsov, Y. A., Sandstede, B. and Wang, X., 1998. *AUTO 97*. Concordia University, Montreal, Canada.

Luongo, A., Rega, G. and Vestroni, F., 1989. “Non-resonant non-planar free motions of inextensional non-compact beams”. *Journal of Sound and Vibration*. Vol. 134, No. 1, p. 73-86.

Nayfeh, A.H. and Pai, P.F., 1989. “Nonlinear nonplanar parametric responses of an inextensional beam”. *International Journal of Non-Linear Mechanics*. Vol. 24, p. 139-158.

Pai, P.F. and Nayfeh, A.H., 1990. “Nonlinear nonplanar oscillations of a cantilever beam under lateral base excitations”. *International Journal of Non-Linear Mechanics*. Vol. 25, p. 455-474.

Zaretzky, C.L. and Crespo da Silva, M.R.M., 1994. “Experimental investigation of non-linear modal coupling in the response of cantilever beams”. *Journal of Sound and Vibration*. Vol. 174, p. 145-167.

9. RESPONSIBILITY NOTICE

The authors are the only responsible for the printed material included in this paper.